PHYSICAL REVIEW B **80**, 241105(R) (2009)

Superelastic metal-insulator phase transition in single-crystal VO_2 nanobeams

W. Fan,[1,2] S. Huang,[1] J. Cao,[1,3] E. Ertekin,[4,5] C. Barrett,[1,3] D. R. Khanal,[1,3] J. C. Grossman,[5] and J. Wu[1,3,4,*]

[1]*Department of Materials Science and Engineering, University of California, Berkeley, Berkeley, California 94720, USA*

[2]*Department of Thermal Science and Energy Engineering, University of Science and Technology of China, Hefei, China*

[3]*Materials Sciences Division, Lawrence Berkeley National Laboratory, Berkeley, California 94720, USA*

[4]*Berkeley Nanosciences and Nanoengineering Institute, University of California, Berkeley, Berkeley, California 94720, USA*

[5]*Department of Materials Science and Engineering, Massachusetts Institute of Technology, 77 Massachusetts Avenue, Cambridge, Massachusetts 02139-4307, USA*

(Received 9 October 2009; published 11 December 2009; corrected 16 December 2009)

We investigated external-stress-induced metal-insulator phase transitions in cantilevered single-crystal VO_2 nanobeams at variable temperatures using a combined theoretical and experimental approach. An atomic force microscope was used to measure the force-displacement curve of the nanobeams, which showed nonlinearity that signifies activation and expansion of domains of a new phase out of the old one. Superelasticity of the VO_2 nanobeam and supersaturation of the phase transition were clearly observed and quantified within the general theory of first-order phase transitions. Phase field modeling was employed to understand the energetics of the domain formation.

DOI: 10.1103/PhysRevB.80.241105 PACS number(s): 71.30.+h, 62.20.−x, 72.80.Ga

First-order phase transitions are characterized by a discontinuity in the first derivative of free energy and are of great interest in materials science, physics, and chemistry. Dynamically probing the transition in the phase space of pressure (P), temperature (T) and volume (V) helps to reveal the fundamental mechanism underlying the phase transition. A good example is the condensation-evaporation process between a liquid and its vapor. When the vapor is compressed isothermally below the critical temperature, P first increases following the ideal gas law, then reaches a plateau where liquid droplets nucleate out of the vapor forming a liquid-vapor coexisting system. In this coexisting state the compressibility of the system diverges because the decrease in total V is accounted for by the conversion of more vapor into denser liquid rather than to increase P as in the pure ideal gas. After completion of the transition, P increases sharply with further reduction in V due to the low compressibility of the liquid.[1] On the other hand, on the P-T curve for the liquid-vapor coexisting system, the slope is directly related to the enthalpy change (latent heat, ΔH) of the phase transition by the Clapeyron equation.

These analyses are universally applicable to all first-order phase transitions. First-order solid-solid phase transitions are expected to have similar isotherms as in the conventional vapor-liquid phase transition. However, the transition dynamics are not easily accessible due to the small change in volume between these phases and extremely high pressure needed experimentally to drive the transition. Previous work has been largely focused on the reversible transformation between the austenitic and martensitic phases of shape memory alloys.[2,3] Their elastic properties are remarkably modified by the reversible motion of domain boundaries, an effect known as superelasticity,[2] similar to the divergent compressibility of the vapor-liquid coexisting system.

This effect has been recently suggested in the first-order metal-insulator phase transition (MIT) of VO_2.[4,5] In the strain-free state, VO_2 undergoes the MIT at $T_C^0 = 341$ K with a change in conductivity of several orders of magnitude.[6,7] The MIT is accompanied by a structural phase transition from the high-temperature tetragonal phase [metallic (M)] to the low-temperature monoclinic phase [insulating (I)], where the sample expands along the tetragonal c-axis direction by $\varepsilon_0 \approx 1\%$.[7–9] As detailed in a previous work, a uniaxial compressive (tensile) stress along this direction drives the system toward the M (I) phase,[5] where the critical stress (σ) needed to trigger such transition at temperature T_C follows the uniaxial Clapeyron equation,

$$\frac{dT_C}{d\sigma} = \frac{\varepsilon_0 T_C^0}{\Delta H}. \tag{1}$$

Our previous work has established the σ-T phase diagram for VO_2 by measuring the MIT behavior of stressed VO_2 microbeams at elevated temperatures.[5] In the recent work of Wei *et al.*,[4] a VO_2 microbeam is clamped at its two ends with fixed length L, such that the beam is forced to move along the M-I phase boundary line when temperature is varied, a process analogous to the isochoric (P-T at fixed V) process of a vapor-liquid system. Interesting physics has been discovered such as a constant free-electron density along the M-I boundary line and a mechanical signature of the MIT.[4] These discoveries are essential for better understanding the physics of the MIT in VO_2, which belongs to the class of so-called strongly correlated electron materials.[10] It has been long debated whether the MIT in VO_2 is primarily a Mott transition or a Peierls transition,[7,11] and Wei *et al.*'s results seem to suggest the former. Owing to the intrinsic coupling between their structural and electronic degrees of freedom, strongly correlated electron materials can be better understood when their mechanical and electromechanical properties are investigated in analogy to those in the vapor-liquid system. To further elucidate the MIT physics in VO_2, it is much desired to probe the isothermal (P-V at fixed T) behavior of the MIT so that a complete picture can be drawn in its three-dimensional σ-L-T phase diagram (in analogy to the P-V-T diagram of the vapor-liquid system). However, dynamically varying the length of a solid up to the critical strain ($\sim \pm 2\%$) is difficult as the material response can be easily dominated by non-uniform strain distribution and/or micro-

scopic fracturing. Nanoscale single crystals, on the other hand, are susceptible to extraordinarily large and uniform strain without fracture due to their small number of structural defects compared to bulk specimens.[5] In this work we synthesized single-crystal VO_2 nanobeam cantilevers and investigated their stress-strain response by mechanically activating and probing the MIT along the nanobeams with an atomic force microscope (AFM). We observed clear superelastic behavior of the VO_2 nanobeams caused by the nucleation and growth of new domains across the MIT. Other properties such as elastic modulus and supersaturation are also quantified. Phase-field simulations were used to confirm that superelastic behavior is expected for the nanobeam geometries and material properties under consideration and reproduced effectively the force-displacement data obtained in experiment. These findings provide a full picture of the electromechanical properties of VO_2 and lend insight on the physics of its MIT.

Single-crystalline VO_2 nanobeams and microbeams were synthesized using the vapor transport method reported previously.[12,13] These beams grow along the tetragonal c axis with {110} planes as bounding side faces.[12] Here the VO_2 beams of interest grew out of the edge of the SiO_2/Si substrate, with one portion firmly bottom-clamped on the substrate during the high-temperature growth and the other portion free standing, naturally forming a cantilever, as shown in Fig. 1(a). When temperature is near T_C^0, the clamped portion shows multiple *M-I* domains as a result of strain accumulated along the beam imposed by the elastically mismatched substrate.[13] The cantilevered portion, on the other hand, is strain free and therefore exhibits single domain behavior, namely, abruptly switches from *I* phase (bright reflection) at $T<T_C^0$ to *M* phase (dark reflection) at $T>T_C^0$, also shown in Fig. 1(a).

An AFM was used to probe the mechanical behavior of these cantilevered VO_2 nanobeams. The AFM tip was in contact with the VO_2 beam at a force location of a away from the clamping root, and force (f)-displacement (w) curves were recorded by pushing the nanobeam downward at a loading-unloading frequency of 0.1 Hz.[14] The spring constant of the AFM tip ($k_{tip}=36$ N/m) was calibrated using a reference cantilever, and the force location was measured from the root using tapping mode scanning.

Figure 1(c) shows representative f-w curves of the VO_2 nanobeam shown in Fig. 1(a) recorded at various temperatures. At small deflections, the f-w curve is linear as expected. At large deflections (but still within the reversible elastic regime), the f-w curves deviates from the initial slope and shows strong nonlinearity evidenced by kinks, as seen in Fig. 1(c). These kinks are reproducible upon repeated bending of the VO_2 nanobeam, and occur at lower w at temperatures that are closer to T_C^0. At the same degree of deflection, no such kinks were observed when bending nanobeams with similar size but made of materials without phase transition, such as ZnO (not shown).

According to elastic theory, the differential equation that governs the deflection of a beam in small-angle deformation is[15]

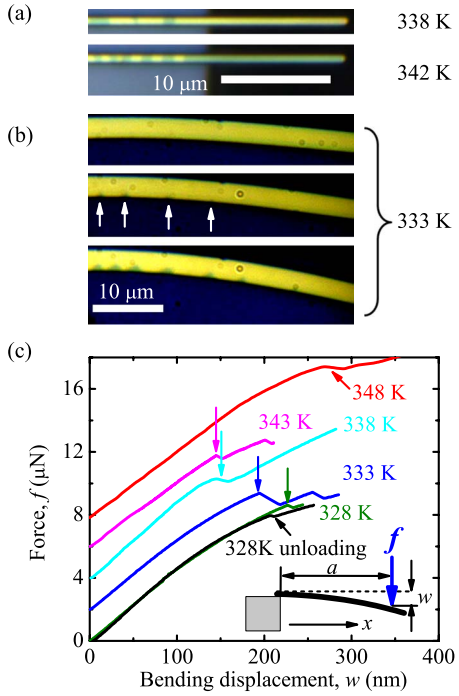

FIG. 1. (Color online) (a) Optical images (top view) of a cantilevered VO_2 nanobeam grown out of the edge of quartz substrate taken at temperatures slightly below (338 K) and above (342 K) the natural MIT temperature. (b) Optical images of side bending a VO_2 microbeam one-end clamped on substrate, showing an array of triangular *M* domains nucleating and evolving at the root of the microbeam with increasing bending curvature. Arrows indicate small *M* domains growing out of the *I* phase. (c) Force-displacement curves of a VO_2 cantilever measured at various temperatures. The curves are vertically offset for clarity. The VO_2 is a beam of height $h=800$ nm and width $b=1100$ nm. The force location is $a=7$ μm. Arrows shows the position of first slope change or kink on each curves. Inset shows a schematic of the geometry.

$$YId^2w/dx^2 = f(a-x), \tag{2}$$

where Y is the Young's modulus and $I=bh^3/12$ is the moment of inertia (b is the width and h is the height of the beam). Solving the equation for f as a function of w, one can define an effective spring constant of the beam, $k_{beam}=f/w=3YI/a^3$. The strain profile across the beam is given by $\varepsilon(\xi,x)=3w\xi(a-x)/a^3$, where ξ is the distance between the point of interest and the neutral plane in the beam. Therefore, the top (bottom) edge of the bent beam at its root (i.e., the clamped end), where $\xi=\pm h/2$, $x=0$, is under maximum tensile (compressive) stress.

The kinks on the f-w curves in Fig. 1(c) signify the onset of the stress-induced MIT at the root of the VO_2 nanobeam. At temperatures lower than T_C^0, the bottom edge at the root of the nanobeam will be compressively stressed with increasing bending. At a critical compressive stress, new *M* domains start to nucleate out of the original *I* phase, and the bottom portion of the nanobeam root enters an *M-I* phase coexisting state. As the nanobeam is further bent beyond the critical stress, the *M* domains start to grow in response to the increasing compression. Similar to the divergent compressibil-

ity for the vapor-liquid coexisting system, a vanishing Young's modulus is expected from the *M*-*I* coexisting part (bottom portion) of the nanobeam. The top portion of the nanobeam, however, is under tension and therefore remains in the original *I* phase. The overall Young's modulus measured is the effective Young's modulus of the composite beam consisting of these two elastically coupled portions across the neutral plane along the nanobeam. This explains the lower but nonzero slope of the *f*-*w* curves beyond the first kink (superelastic regime). At temperatures higher than T_C^0, similar scenario exists except that now new *I* domains nucleate out of the *M* phase in the top portion of the nanobeam as a result of the maximum tensile stress there, while the bottom portion remains *M* phase.

In order to visualize the domain nucleation and growth process, we bend another wider VO_2 microbeam sidewise and simultaneously image the beam using a high-magnification optical microscope. Figure 1(b) shows the optical images of such a beam slightly below T_C^0. It can be seen that at certain critical stress, an array of triangular *M* domains (dark) evolve out of the *I* phase (bright) at the compressive portion near the root. With increasing bending, these *M* domains grow in size at a speed that is much faster than the bending speed, such that the domains always stay in an equilibrium configuration during the bending. At large bending displacements, new domains also emerge at different locations in addition to the old domains growing. The nucleation of these new domains may be responsible for the second kink seen on some of the *f*-*w* curves in Fig. 1(c).

We calculate the critical stress from the first kink on the *f*-*w* curves and plot on the stress-temperature phase diagram in Fig. 2(a). The *M*-*I* phase boundary, as denoted by the dashed line, is calculated from the Clapeyron equation using a latent heat of the MIT of 1020 Cal/mol.[6,16] The measured critical stress points are distributed along the phase boundary line, consistent with the Clapeyron equation and showing supercompressing ($T<T_C^0$) and superstretching ($T>T_C^0$) effects in Fig. 2(a). We also calculated the Young's modulus (Y) of VO_2 from the linear part of the *f*-*w* curve at small *w* at different temperatures[14] [Fig. 2(b)]. Y is found to be constant over the full temperature range and equal to 155 ± 15 GPa, compared to previously reported 140 GPa for VO_2 thin films.[17,18] The effective Young's modulus after in the superelastic regime is also calculated and labeled as Y_{super} and plotted together with Y in Fig. 2(b).

To illustrate further that the phase coexistence mechanism described here is sufficient to explain the slope changes observed on the *f*-*w* curves, the phase field approach has been applied to understand the energetics of domain dynamics. In the approach implemented here, the coupled phase ϕ and displacement fields are determined self-consistently on a two-dimensional grid corresponding to a planar surface of the beam with the *x* direction along the beam axis and the *y* direction along the beam height. The phase variable ϕ varies from 0 (*I* phase) to 1 (*M* phase). The phase field is evolved from an initial random distribution via Cahn-Allen dynamics such that the total energy given by

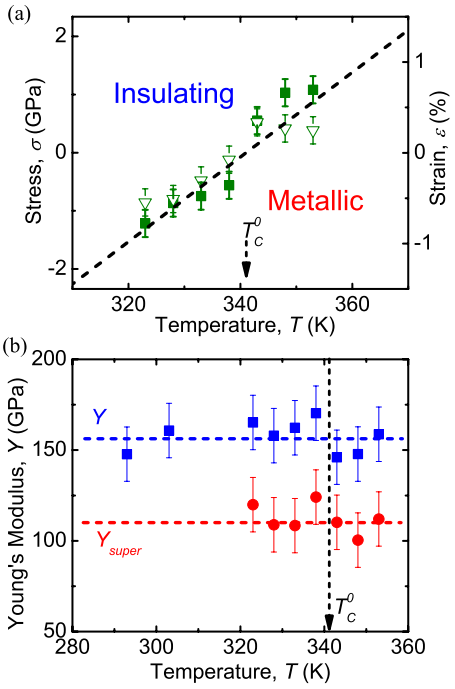

FIG. 2. (Color online) (a) Calculated stress at the root of the VO_2 beam at the measured first kink of the force-displacement curves plotted in the stress-temperature phase space. Solid squares and empty triangles represent the stress in the loading and unloading process, respectively. The dashed line is the phase boundary calculated from the Clapeyron equation using a latent heat $\Delta H = 1020$ Cal/mol. (b) Young's modulus of the VO_2 beam measured as a function of temperature in the elastic (squares) and superelastic (circles) regimes.

$$F(\phi) = \int \left\{ f(\phi) + \frac{\beta^2}{2}|\nabla\phi|^2 + \frac{1}{2}C_{ijkl}[\varepsilon_{ij} - \varepsilon_{ij}^T(\phi)][\varepsilon_{kl} - \varepsilon_{kl}^T(\phi)] \right\} dA \quad (3)$$

is minimized;[19] all spatial derivatives are computed numerically via second-order central finite differences, while the temporal evolution of the phase field occurs via first-order forward integration. In the expression above, the double-well potential $f(\phi)$ describes the relative thermodynamic energy of the *M* and *I* phases and depends on temperature.[20] The second term reflects the interfacial energy, which is taken as isotropic here with the parameter β chosen so that the total energy across an interface corresponds approximately to 25 mJ/m^2.[13] The last term represents the elastic energy where C is the elastic modulus tensor, ε is the geometric strain, and ε^T is the transformation strain between the two phases: $\varepsilon_{xx}^T(\varphi)$ varies smoothly from 0 to $-\varepsilon_0=-0.01$ as ϕ varies from 0 to 1, and $\varepsilon_{xy}^T=\varepsilon_{yy}^T=0$ for all values of ϕ. As the phase field is evolved, the elastic fields are simultaneously relaxed according to the finite-difference equations of mechanical equilibrium, which are solved via direct matrix inversion. The scheme continues until the coupled displacement and phase fields are obtained self-consistently. Boundary conditions corresponding to the deflection of a fixed-free beam with a specified terminal load are applied.

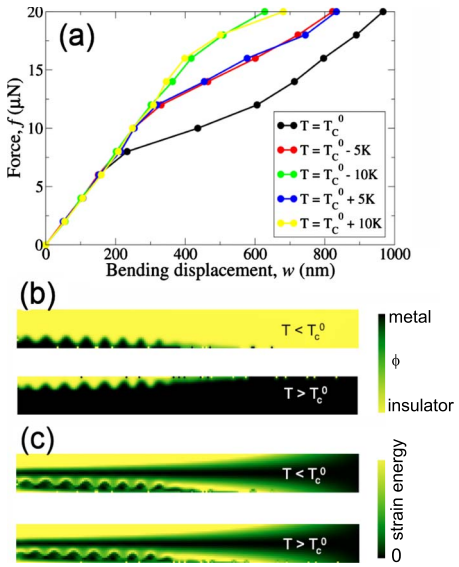

FIG. 3. (Color online) (a) Simulated force-displacement curves for a nanobeam demonstrating the slope change that occurs at the onset of new domain formation. (b) Domain distribution obtained by two-dimensional phase field simulation incorporating local strain relaxation for a beam of length 7.5 μm and height 0.75 μm. The applied terminal load force is 20 μN, for temperatures below and above the natural transition temperature, respectively. (c) Residual strain energy distributions corresponding to the parameters in part (b) illustrating how new domains relieve strain energy.

The temperatures are chosen so that the difference in the thermodynamic Gibbs free energies of the *M* and *I* phases are consistent with a latent heat of 1020 Cal/mol and an entropy change of 2.99 Cal/mol K.[21] The final vertical displacement at the free end of the beam is recorded for different applied loads at different temperatures, and in Fig. 3(a) the computed *f*-*w* curves are shown. These curves are qualitatively similar in nature to those obtained experimentally, exhibiting a slope change associated with the superelasticity that occurs at the onset of new phase nucleation. The final phase distribution and residual strain energy are shown in Figs. 3(b) and 3(c) for forces corresponding to the onset of *M* domains nucleation and larger. In the simulations, nucleation occurs initially where the compression is the largest at the fixed end of the beam. As the force applied is increased, the *M* phase grows in response and extends along the beam axis. The onset of the new phase occurs earlier at the transition temperature and later at temperatures away from the transition temperature, in agreement with experimental observations in Fig. 2(a). However, only thermodynamic equilibrium states are considered in the modeling, therefore the exact domain configuration [Fig. 1(b)] and the supersaturation effects [Fig. 2(a)] in experiments are not described by the modeling.

In summary, by bending a cantilevered single-crystal VO_2 nanobeam with an AFM, we mechanically activated and probed the metal-insulator phase transition at various temperatures. Superelastic and supersaturation behavior of the transition corresponding to nucleation and growth of domains of new phase out of the old phase were clearly observed and quantified. These results were discussed in the general framework of first-order phase-transition theory. The equilibrium domain structure was simulated by minimizing the total energy of the system using phase field modeling.

The sample preparation in this work was supported by National Science Foundation under Grant No. EEC-0425914 and the device fabrication and characterization by the Laboratory Directed Research and Development Program of Lawrence Berkeley National Laboratory under the Department of Energy Contract No. DE-AC02-05CH11231. J.C.G. and E.E. acknowledge funding by the Focus Center Research Program on Materials, Structures, and Devices (FCRP/MSD).

*Author to whom correspondence should be addressed; wuj@berkeley.edu

[1] D. A. McQuarrie and J. D. Simon, *Physical Chemistry: A Molecular Approach* (University Science Books, Sausalito, 1997).
[2] J. S. Juan, M. L. No, and C. A. Schuh, Nat. Nanotechnol. **4**, 415 (2009).
[3] K. Otsuka and C. Wayman, *Shape Memory Materials* (Cambridge University Press, New York, 1999).
[4] J. Wei, Z. Wang, W. Chen, and D. H. Cobden, Nat. Nanotechnol. **4**, 420 (2009).
[5] J. Cao, E. Ertekin, V. Srinivasan, W. Fan, S. Huang, H. Zheng, J. W. L. Yim, D. R. Khanal, D. F. Ogletree, J. C. Grossman, and J. Wu, Nat. Nanotechnol. **4**, 732 (2009).
[6] C. N. Berglund and H. J. Guggenheim, Phys. Rev. **185**, 1022 (1969).
[7] V. Eyert, Ann. Phys. **11**, 650 (2002)
[8] M. Marezio, B. McWhan, P. D. Dernier, and J. P. Remeika, Phys. Rev. B **5**, 2541 (1972).
[9] J. C. Rakotoniaina, R. Mokranitamellin, J. R. Gavarri, G. Vacquier, A. Casalot, and G. Calvarin, J. Solid State Chem. **103**, 81 (1993).
[10] E. Dagotto, Science **309**, 257 (2005).
[11] S. Biermann, A. Poteryaev, A. I. Lichtenstein, and A. Georges, Phys. Rev. Lett. **94**, 026404 (2005).
[12] B. S. Guiton, Q. Gu, A. L. Prieto, M. S. Gudiksen, and H. Park, J. Am. Chem. Soc. **127**, 498 (2005).
[13] J. Wu, Q. Gu, B. S. Guiton, N. de Leon, O. Lian, and H. Park, Nano Lett. **6**, 2313 (2006).
[14] M. J. Gordon, T. Baron, F. Dhalluin, P. Gentile, and P. Ferret, Nano Lett. **9**, 525 (2009).
[15] S. Timoshenko, *Strength of Materials: Part I* (Van Nostrand, New York, 1940).
[16] O. A. Cook, J. Am. Chem. Soc. **69**, 331 (1947).
[17] K. Y. Tsai, T. S. Chin, and H. P. D. Shieh, Jpn. J. Appl. Phys., Part 1 **43**, 6268 (2004).
[18] N. Sepúlveda, A. Rua, and R. Cabrera, Appl. Phys. Lett. **92**, 191913 (2008).
[19] J. J. Eggleston, G. B. McFadden, and P. W. Voorhees, Physica D **150**, 91 (2001).
[20] T. Biben, Eur. J. Phys. **26**, S47 (2005).
[21] P. Schilbe and D. Maurer, Mater. Sci. Eng., A **370**, 449 (2004).